Polymer 51 (2010) 3493–3502

Contents lists available at ScienceDirect

Polymer

journal homepage: www.elsevier.com/locate/polymer

Synthesis and micelle behavior of (PNIPAm-P*t*BA-PNIPAm)$_m$ amphiphilic multiblock copolymer

Binyang Du [a,*], Aixiong Mei [a], Yong Yang [a], Qinfen Zhang [b], Qi Wang [a], Junting Xu [a], Zhiqiang Fan [a]

[a] MOE Key Laboratory of Macromolecular Synthesis and Functionalization, Department of Polymer Science & Engineering, Zhejiang University, Hangzhou 310027, China
[b] BioEM lab, State Key Lab of Biocontrol, School of life Sciences, Sun Yat-Sen University, Guangzhou 510275, China

ARTICLE INFO

Article history:
Received 3 December 2009
Received in revised form
29 May 2010
Accepted 2 June 2010
Available online 9 June 2010

Keywords:
Amphiphilic
Multiblock copolymer
Micelle

ABSTRACT

A linear amphiphilic multiblock copolymer (PNIPAm-P*t*BA-PNIPAm)$_m$ was successfully synthesized by a two-step reversible addition–fragmentation transfer (RAFT) polymerization in the presence of a cyclic trithiocarbonate as RAFT agent. The micelle behavior of (PNIPAm-P*t*BA-PNIPAm)$_m$ multiblock copolymer in aqueous solution was then investigated by means of normal TEM, cryo-TEM, static and dynamic light scattering. The morphology, size, and size distribution of (PNIPAm-P*t*BA-PNIPAm)$_m$ micelles were found to be dependent on the initial concentration of multiblock copolymer in THF. Spherical micelles, associated aggregates of spherical micelles, cage-like micelles, layered structures, and vesicular micelles were experimentally observed, which were in good agreement with the prediction of theory and simulations on linear amphiphilic multiblock copolymer in selective solvent. The (PNIPAm-P*t*BA-PNIPAm)$_m$ micelles also exhibit thermo-sensitive behavior in aqueous solution because of the PNIPAm blocks.

1. Introduction

The micelle behavior of amphiphilic block copolymers in solutions is a long-stand hot topic in polymer physics [1–8]. During the past decades, the micelle behavior and morphology of amphiphilic diblock and triblock copolymers in selective solvents have been extensively studied [9–15]. Nowadays, the formation of micelles, morphology of micelles and even their evolution partway of diblock and triblock copolymers in selective solvents can be controlled to certain extent by balancing the energies among the stretching of the core-forming block, the interfacial tension between the core and the solvent outside the core region, and the repulsion among the corona chains [11,16–20].

With the development of new synthetic methods, more attentions are recently paid to the synthesis of amphiphilic multiblock copolymers and their micelle behavior in selective solvents, which is expected to be more complex [21–27]. Understanding of micelle behavior of multiblock copolymers is thus thought to be a new challenge for polymer physicists. In fact, in early 90s Halperin et al. had considered the micelle behavior of multiblock copolymer in selective solvent from a theoretical point of view and predicted that a flowerlike single intramolecular micelle or a string of molecular micelles may be formed [28]. By employing static and dynamic light scattering, the formation of flowerlike micelles was confirmed for a pentablock copolymer of $(D_{20}$-*b*-$M_{10})_3$ in aqueous solution [21]. Here, D and M stand for 2-(dimethylamino)ethyl methacrylate and methyl methacrylate, respectively [21]. For pseudo-multiblock copolymer poly(N-isopropylacrylamide-*s*-styrene) chains with evenly spaced hydrophobic styrene segments, Zhang et al. observed that these copolymer chains form single-flowerlike core-shell nanoparticles in aqueous solution at temperature ~30.6 °C [29]. For double hydrophilic multiblock copolymers of *N,N*-dimethylacrylamide and *N*-isopropylacrylamide, (PDMAm$_p$-PNIPAm$_q$)$_m$ in aqueous solution, flowerlike unimolecular and multimolecular micelles were observed by heating the solution temperature above the LCST of PNIPAm. However, these experimental studies are mostly focused on using light scattering techniques to probe the micelle structures of multiblock copolymers in their dilute solution [22–25]. Visible micelle morphologies of multiblock copolymer in selective solvents are rare reported [26,27].

Simulations had also been used to study the micelle behavior of multiblock copolymers and various micelle structures were obtained under different simulation models [30–32]. Among them, in a recent three-dimensional Monte Carlo simulation of dilute solutions of amphiphilic multiblock copolymers with a large number of blocks, micelles, chains of micelles, tubes, and layered structures were found, which were dependent on the ratio of hydrophobic to hydrophilic block lengths and the quality of the solvent [32]. The simulation results indicate the complex micelle behavior and rich micelle morphologies of multiblock copolymers

* Corresponding author. Tel.: +86 571 87953164; fax: +86 571 87952400.
E-mail address: duby@zju.edu.cn (B. Du).

0032-3861/$ – see front matter © 2010 Elsevier Ltd. All rights reserved.
doi:10.1016/j.polymer.2010.06.007

in selective solvents. More experiments are thus strongly required to testify the theoretical and simulation predications and further understand the micelle behavior of multiblock copolymers in selective solvents.

In the present work, a linear amphiphilic multiblock copolymer (PNIPAm-P*t*BA-PNIPAm)$_m$ was synthesized by a two-step reversible addition–fragmentation transfer (RAFT) polymerization in the presence of a cyclic trithiocarbonate as RAFT agent. Normal TEM and cryo-TEM were employed to directly visualize the morphologies of (PNIPAm-P*t*BA-PNIPAm)$_m$ micelles formed in aqueous solution, which is a selective solvent for hydrophilic PNIPAm blocks. The ensemble properties of (PNIPAm-P*t*BA-PNIPAm)$_m$ micelle solutions were investigated by static and dynamic light scattering. The experimental results were discussed and correlated with the predictions of theoretical and simulation studies.

2. Experimental section

2.1. Chemical and materials

N-isopropylacrylamide (NIPAm: 99%, ACROS ORGANICS) was purified by recrystallization from *n*-hexane. *t*-Butyl acrylate (*t*-BA, ACROS ORGANICS) was dried over CaH_2 overnight and distilled under reduced pressure. 1,4-dioxane (Shanghai Chemical Reagent) was dried by refluxing in the presence of sodium flakes and distilled prior to use. The initiator, α,α′-azodiisobutyronitrile (AIBN) was recrystallized from methanol. All other reagents were of analytical grade and used as received.

2.2. Synthesis of $(PtBA)_n$ multiblock polymer

The poly(*t*-butyl acrylate) multiblock polymer, (P*t*BA)$_n$, was synthesized by reversible addition–fragmentation transfer (RAFT) polymerization in the presence of a cyclic trithiocarbonate, 4,7-diphenyl -[1,3]dithiolane-2-thione, (DPDTT) [33–36]. Briefly, *t*-butyl acrylate (3 ml), AIBN (5 mg), and DPDTT (50 mg) were charged into an ampule. After the complete dissolution of AIBN and DPDTT, the ampule was degassed with three freezing–evacuation–thawing cycles, sealed, and put in an oil bath with preset temperature of 80 °C for polymerization. The polymerization was stopped after 6 h and the rough product was dissolved with THF. The polymer was precipitated with methanol/H_2O (1/1) mixture and then centrifuged, filtered and dried in vacuum at 40 °C. The final (P*t*BA)$_n$ multiblock polymer was ca. 1.99 g with yield of ca. 66.7%.

2.3. Synthesis of $(PNIPAm\text{-}PtBA\text{-}PNIPAm)_m$ multiblock copolymer

The (PNIPAm-P*t*BA-PNIPAm)$_m$ multiblock copolymer was synthesized by RAFT polymerization with (P*t*BA)$_n$ multiblock polymer as macromolecular RAFT agent. Briefly, (P*t*BA)$_n$ multiblock polymer (0.5 g), NIPAm (1 g), AIBN (2 mg), and dioxane (3 ml) were charged into an ampule. After the complete dissolution of (P*t*BA)$_n$, NIPAm, and AIBN, the ampule was degassed with three freezing–evacuation–thawing cycles, sealed, and put in an oil bath with preset temperature of 80 °C for polymerization. The polymerization was stopped after 6 h and the rough product was dissolved with THF. The polymer was precipitated with methanol/H_2O (1/1) mixture and then centrifuged, filtered and dried in vacuum at 40 °C. The (PNIPAm-P*t*BA-PNIPAm)$_m$ multiblock copolymer was ca. 1.14 g with yield of ca. 76%.

2.4. Cleavage of $(PtBA)_n$ multiblock polymer

The (P*t*BA)$_n$ multiblock polymer was cleaved with excess amount of AIBN in dioxane at 80 °C under nitrogen. 0.1g (P*t*BA)$_n$, 50 mg AIBN, and 5 ml dioxane were charged into an ampule and then reacted at 80 °C under nitrogen and vigorously stirring for 24 h. After cooling to room temperature, 1:1 methanol/H_2O mixture was used to precipitate the resultant P*t*BA, which was then dried in vacuum.

2.5. Cleavage of $(PNIPAm\text{-}PtBA\text{-}PNIPAm)_m$ multiblock copolymer

0. 1 g (PNIPAm-P*t*BA-PNIPAm)$_m$, 50 mg AIBN, and 5 ml dioxane were charged into an ampule and then reacted at 80 °C under nitrogen and vigorously stirring for 24 h. After cooling to room temperature, the resultant PNIPAm-P*t*BA-PNIPAm triblock copolymer was precipitated by 1:1 methanol/H_2O mixture and then dried in vacuum. Scheme 1 briefly schematizes the synthetic route and the structures of the (PNIPAm-P*t*BA-PNIPAm)$_m$ multiblock copolymer.

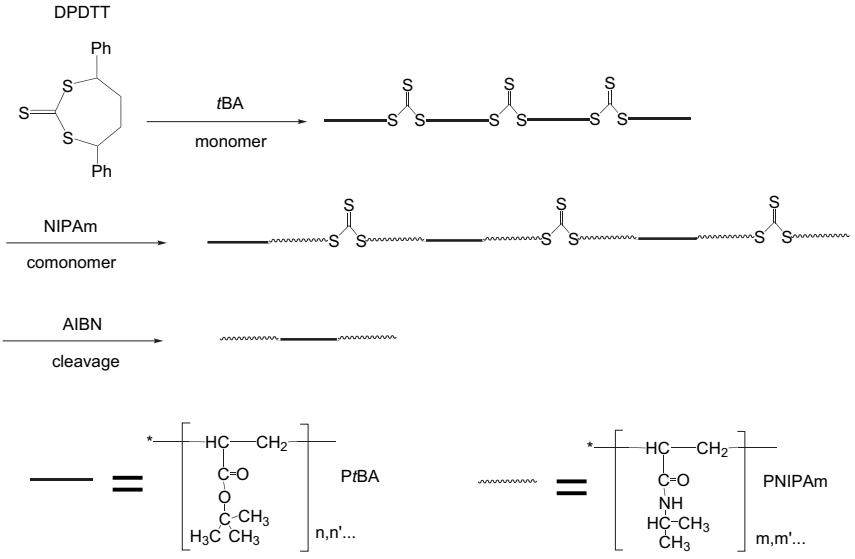

Scheme 1. The synthetic route and the structure of the (PNIPAm-P*t*BA-PNIPAm)$_m$ multiblock copolymer and the corresponding triblock copolymer after cleavage in dioxane with excess AIBN.

2.6. Determination of critical micelle concentration (CMC) of (PNIPAm-PtBA-PNIPAm)$_m$

15.2 mg (PNIPAm-P*t*BA-PNIPAm)$_n$ multiblock copolymer was dissolved in 250 ml distilled water to give the stock solution with concentration of 0.06 mg/ml. Afterward, four solutions with 0.04 mg/ml, 0.03 mg/ml, 0.02 mg/ml, and 0.01 mg/ml were prepared from this stock solution by dilution. The other five solutions with 0.008 mg/ml, 0.006 mg/ml, 0.004 mg/ml, 0.002 mg/ml and 0.001 mg/ml were then prepared from the 0.01 mg/ml solution by dilution.

12.7 mg pyrene was dissolved in 50 ml acetone to give a concentration of ca. 1.26×10^{-3} mol/l. Each of the ten clean volumetric glass flasks (10 ml) was charged with an aliquot (4 μl) of such pyrene acetone solution, respectively, and then dried with nitrogen. Afterward, 10 ml of the above prepared (PNIPAm-P*t*BA-PNIPAm)$_m$ aqueous solutions with various concentration were added into these flasks, respectively. The final pyrene concentration in the multiblock copolymer solution was about 5×10^{-7} mol/L. The fluorescence excitation spectra of the (PNIPAm-P*t*BA-PNIPAm)$_m$-pyrene aqueous solutions were measured by luminescence spectrometer.

2.7. Preparation of (PNIPAm-PtBA-PNIPAm)$_m$ micelle

The (PNIPAm-P*t*BA-PNIPAm)$_m$ multiblock copolymer was first dissolved in tetrahydrofuran (THF) to obtain homogeneous solutions with concentrations of 0.25 wt.%, 0.1 wt.%, 0.05 wt.%, and 0.025 wt.%, respectively. The concentrations used here were well above the CMC concentration of the multiblock copolymer (PNIPAm-P*t*BA-PNIPAm)$_m$ in aqueous solution, which allows the formation of (PNIPAm-P*t*BA-PNIPAm)$_m$ micelles in aqueous solution. To obtained micelle, distilled water was drop-wisely (ca. 1 droplet per 10 s) added into the 3 ml copolymer THF solutions under vigorously magnetic stirring. The addition of water was continued until the desired water content (20 wt.%) was reached. The mixing solutions were then transferred to dialysis tubes with molecular cut-off of 3500 and dialyzed against distilled water for 3 days at room temperature in order to completely get rid of THF. The distilled water was frequently changed during the dialysis process. The obtained micelle aqueous solutions were transferred into clean volumetric glass flasks. The (PNIPAm-P*t*BA-PNIPAm)$_m$ micelles were stable in aqueous solutions for more than two months. The obtained micelles were then subjected to further characterization.

2.8. Instruments and characterization

Number average and weight average molecular weights (M_n and M_w) and molecular weight distributions of (PNIPAm-P*t*BA-PNIPAm)$_m$ and (P*t*BA)$_n$ multiblock polymers as well as the corresponding cleaved counterparts were determined by gel permeation chromatograph (GPC, PL-GPC 220, Polymer Laboratories Ltd.) with tetrahydrofuran as the eluent and monodisperse polystyrene as the calibration standard. ^{1}H NMR of the copolymers was performed on a 300 MHz Varian Mercury Plus NMR instrument with $CDCl_3$ as solvent and tetramethylsilane (TMS) as internal standard.

Fluorescence measurements were performed on a PerkinElmer LS55 luminescence spectrometer with 1 cm quartz cells. Excitation spectra of the (PNIPAm-P*t*BA-PNIPAm)$_m$-pyrene samples were obtained with the emission wavelength at 372 nm. The excitation and emission band slits were 3 nm; the intensities of excitation peaks at 339 nm and 333 nm were recorded and plotted as the function of multiblock copolymer concentrations.

The morphologies of the (PNIPAm-P*t*BA-PNIPAm)$_m$ micelles in aqueous solutions were observed with cryogenic (cryo-) and normal transmission electron microscopy (TEM). The cryo-TEM measurements were carried out in the BioEM lab, State Key Lab of Biocontrol, School of life Sciences, Sun Yat-Sen University, Guangzhou, 510275. For cryo-TEM, 4 μl of sample were applied to a holey carbon film grid (R1.2/1.3 Quantifoil Micro Tools GmbH, Jena, Germany), and were absorbed by filter paper (Whatman 1#) for about 3 s. After absorbing, the grid was immediately plunged into pre-cooled liquid ethane for flash frozen. The cryo-grid was held in a Gatan 626 cryo-Holder (Gatan, USA) and transferred intoTEM (JEOL JEM-2010 with 200 KV LaB_6 filament) at −172 °C. The sample was searched and observed under minimal dose condition at −172 °C. The micrographs were recorded by a Gatan 832 CCD camera at the defocus of 3–5.46 μm.

The normal TEM measurements were carried out on a JEOL JEM-1200 electron microscope operated at an acceleration voltage of 60 KV. TEM samples were prepared by dip-coating with Formvar-coated copper grids into the aqueous solutions of (PNIPAm-P*t*BA-PNIPAm)$_n$ micelle. The grids were then stained by 2 wt.% phosphotungstic acid (PTA). The excess solution was gently absorbed away using a strip of filter paper. The grids were then allowed to dry in air at room temperature before observation.

The static and dynamic light scattering (SLS & DLS) of the micelle solutions were carried out on a Brookhaven Instrument BI-200SM with a laser wavelength of 636 nm at 25 °C after the cryo-TEM measurements. The micelle solutions used were the same as those for cryo-TEM imaging. Each dialysis micelle solution was diluted with distilled water to give a total liquid volume of 50 ml.

The thermo-sensitive behavior of the (PNIPAm-P*t*BA-PNIPAm)$_n$ micelles in aqueous solutions was characterized by dynamic light scattering using a 90 Plus Particle Size Analyzer (Brookhaven Instruments Corporation) in the temperature range of 25–50 °C. The scattering angle was 90°. For each temperature, the solution was kept for 15 min to allow equilibrium.

3. Results and discussion

3.1. Syntheses and characterization of (PtBA)$_n$ and (PNIPAm-PtBA-PNIPAm)$_m$

(P*t*BA)$_n$ was successfully synthesized by RAFT polymerization in the presence of DPDTT. Fig. 1 shows the GPC traces of original and cleaved multiblock polymer (P*t*BA)$_n$. The number average molecular weight ($M_{n,o}$) and polydispersity index (PDI$_o$, $M_{w,o}/M_{n,o}$) of the original (P*t*BA)$_n$ multiblock polymer and the corresponding polymer P*t*BA after AIBN cleavage were shown in Table 1. The value of $M_{n,o}/M_{n,t}$ was about 4.56, indicating the success formation of (P*t*BA)$_n$ multiblock polymer. It can be seen that the PDI decreased from 2.36 for (P*t*BA)$_n$ to 1.29 for P*t*BA, which indicates that there is better control of the propagation of the blocks than the whole (P*t*BA)$_n$ multiblock polymer. The molecular weight of P*t*BA after cleavage was closed to the theoretical value. Fig. 2 shows the ^{1}H NMR spectrum of (P*t*BA)$_n$ multiblock polymer and the assignment of the resonances. The resonance peak at 1.38 ppm (a) was attributed to the protons of butyl moieties. The peak at 2.49 ppm (b) was assigned to the methylidyne proton of the P*t*BA backbones.

By using the above obtained (P*t*BA)$_n$ multiblock polymer as macro-RAFT agent and NIPAm as the second monomer, (PNIPAm-P*t*BA-PNIPAm)$_m$ multiblock copolymer was synthesized by RAFT polymerization. Fig. 3 shows the GPC traces of original and cleaved (PNIPAm-P*t*BA-PNIPAm)$_m$ multiblock copolymers. The number average molecular weight ($M_{n,o}$) and polydispersity index (PDI$_o$, $M_{w,o}/M_{n,o}$) of the original (PNIPAm-P*t*BA-PNIPAm)$_m$ multiblock polymer and the corresponding triblock copolymer PNIPAm-P*t*BA-PNIPAm after AIBN cleavage were shown in Table 2. The value of $M_{n,}$

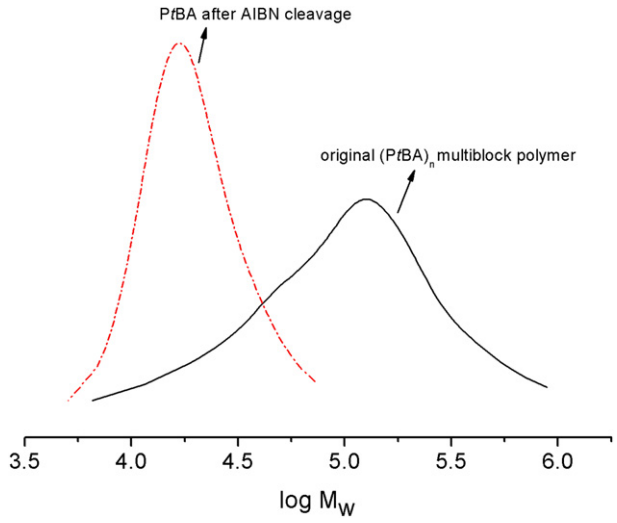

Fig. 1. GPC traces of original and cleaved multiblock polymer $(PtBA)_n$.

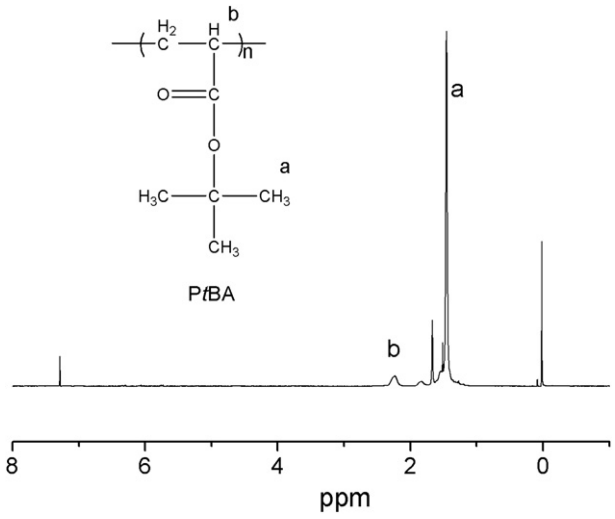

Fig. 2. ^{1}H NMR spectrum of P*t*BA.

$_o/M_{n,t}$ was about 3.61, indicating the success formation of multiblock copolymer. The PDI decreased from 1.96 for original multiblock copolymer to 1.35 for the corresponding triblock copolymer after AIBN cleavage. The GPC results show that the ratio of the numbers of P*t*BA blocks and PNIPAm blocks was about 130:64 ≈ 2.03. Fig. 4 shows the ^{1}H NMR spectrum of (PNIPAm-P*t*BA-PNIPAm)$_m$ multiblock copolymer and the assignment of the resonances. The resonance peak at 1.2 ppm (a) was attributed to the methyl protons of isopropyl amide groups. The peak at 4.2 ppm (b) was assigned to the methylidyne proton of isopropyl groups. The resonance peak at 1.38 ppm (d) was attributed to the protons of butyl moieties. The ratio of the monomer numbers of P*t*BA blocks and PNIPAm blocks was calculated to be about 2.22 from the areas of peaks b and d, which was in excellent agreement with that of 2.03 obtained from the molecular weights of P*t*BA and PNIPAm-P*t*BA-PNIPAm after AIBN cleavage. These results indicate that the successful formation of (PNIPAm-P*t*BA-PNIPAm)$_m$ multiblock copolymer with average *m* of 3–4.

3.2. Critical micelle concentration (CMC) of (PNIPAm-PtBA-PNIPAm)$_m$ aqueous solution

The critical micelle concentration (CMC) of (PNIPAm-P*t*BA-PNIPAm)$_m$ in aqueous solution was determined by using pyrene as a polarity probe [37]. It has been well known that for pyrene, the ratio of intensity of the fluorescence excitation peak at 339 nm and that at 333 nm can be used to characterize the polarity of the probe's environment. The pyrene was then mixed with (PNIPAm-P*t*BA-PNIPAm)$_m$ aqueous solutions with various concentrations and the excitation characteristics of mixed samples were measured with a PerkinElmer LS55 luminescence spectrometer. The intensities of excitation peaks at 339 nm and 333 nm were recorded and the ratio of I_{339}/I_{333} was plotted as the function of multiblock copolymer concentrations, as shown in Fig. 5. Note that the original fluorescence excitation spectra were shown in Fig. S1 (Supporting information). At low concentrations, which were below 0.008 mg/ml, the I_{339}/I_{333} had a plateau value of ca. 0.27. With concentrations above 0.01 mg/ml, I_{339}/I_{333} increased with increasing the copolymer concentrations. The CMC was estimated to be 0.014 mg/ml from the cross-point of the two slopes shown in Fig. 5, which was corresponding to the concentration of 0.0014 wt.% in weight percent. Clearly, the concentrations of (PNIPAm-P*t*BA-PNIPAm)$_m$ solutions used for the preparation of micelles were well above it's CMC. It was expected that (PNIPAm-P*t*BA-PNIPAm)$_m$ form micelles in aqueous solution.

Table 1
Molecular weight and conversion data of *t*BA polymerization in the presence of DPDTT RAFT agent with AIBN as initiator.

Run	Conv.[b] (wt.%)	Original[c]		Treated[d]		Calc.	$M_{n,o}/M_{n,t}$
		$M_{n,o}(10^4)$	PDI_o	$M_{n,t}(10^4)$	PDI_t	$M_{n,R}(10^4)$[e]	
1[a]	66.7	6.80	2.36	1.69	1.29	1.39	4.56

[a] Polymerization condition: 3 mL *t*BA, 50 mg DPDTT and 5 mg AIBN were used, 80 °C tBA/DPDTT/AIBN = 800/5/1.
[b] Conversions were determined gravimetrically.
[c] Number average molecular weight and polydispersity index of original polymer.
[d] Number average molecular weight and polydispersity index of polymer treated with excessive AIBN.
[e] The theoretical number average molecular weights were calculated by the following equation: $M_{n,R}$ = [monomer]/[DPDTT]×Conversion×130.

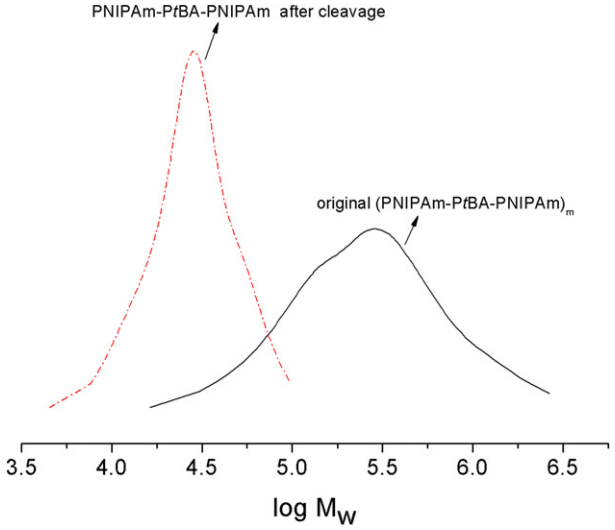

Fig. 3. GPC traces of original and cleaved (PNIPAm-P*t*BA-PNIPAm)$_m$ multiblock copolymers.

Table 2
The number average molecular weight ($M_{n,o}$) and polydispersity index (PDI_o, $M_{w,o}/M_{n,o}$) of (PNIPAm-P*t*BA-PNIPAm)$_m$ multiblock copolymers prepared with (P*t*BA)$_n$ as macro-RAFT agent.

Run	Conv.[b] (wt.%)	Original[c]		Treated[d]		$M_{n,o}/M_{n,t}$
		$M_{n,o}(10^4)$	PDI_o	$M_{n,t}(10^4)$	PDI_t	
2[a]	76	8.74	1.96	2.42	1.35	3.61

[a] Polymerization condition: 0.4g P*t*BA, 1g NIPA, 2 mg AIBN and 3 mL Dioxane were used, 80 °C for 6 h.
[b] Conversions were determined gravimetrically.
[c] Number average molecular weight and polydispersity index of original polymer.
[d] Number average molecular weight and polydispersity index of polymer treated with excessive AIBN.

3.3. Micelle morphology of (PNIPAm-P*t*BA-PNIPAm)$_m$ in aqueous solution

Fig. 6 shows the morphology of (PNIPAm-P*t*BA-PNIPAm)$_m$ micelles in aqueous solution with various initial polymer concentrations obtained by normal TEM. The initial polymer concentration was reported to affect the micelle morphology of linear and cyclic diblock copolymers [38,39]. For cyclic poly(styrene-*b*-isoprene) (PS-PI) copolymer, the micelles formed in heptane (a selective solvent for PI) evolutes from small individual "sunflowerlike" micelles to giant worm-like micelles when the initial PS-PI concentration in heptane increased from 0.01 mg/ml to 5 mg/ml (ca. 0.5 wt.%) [38]. While for linear PS-PI diblock copolymer in heptane, spherical micelles were observed over the range of investigated concentrations [38]. For PS_{410}-PAA_{25} [39], the morphology of micelles in aqueous solution changed from spherical, rod-like micelles into vesicles with increasing the initial copolymer concentration in DMF from 2 wt.% to 4 wt.%. These phenomena were attributed to the dependency of aggregation number on the copolymer concentration [40]. Clearly, the morphology of (PNIPAm-P*t*BA-PNIPAm)$_m$ micelles strongly depends on the initial concentration. It can be seen from Fig. 6 that the micelle morphology of (PNIPAm-P*t*BA-PNIPAm)$_m$ multiblock copolymer in aqueous solutions changes from toroid structures (bilayer and layered structures) at 0.025 wt.% to cage-like structures at 0.05 wt.% and to spherical micelles, as well as their large aggregates at 0.1 wt.% and 0.25 wt.%.

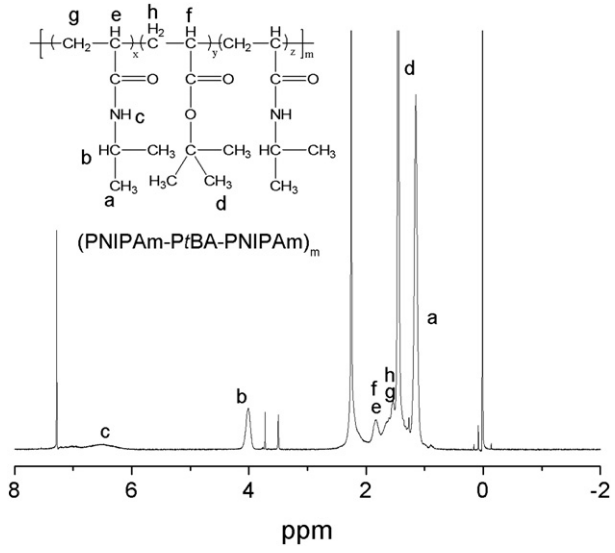

Fig. 4. ^{1}H NMR spectrum of (PNIPAm-P*t*BA-PNIPAm)$_m$.

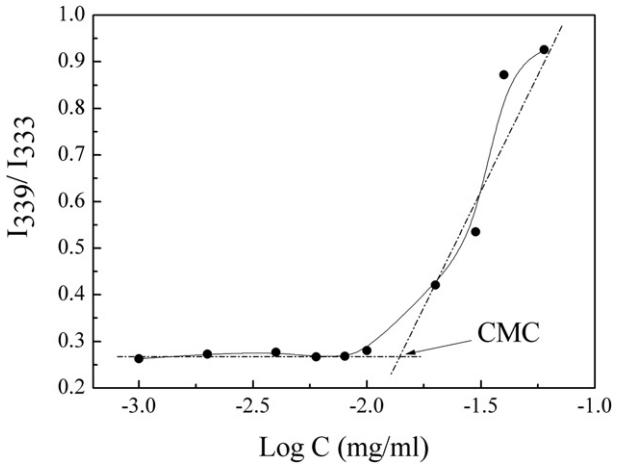

Fig. 5. The ratio of I_{339}/I_{333} as the function of (PNIPAm-P*t*BA-PNIPAm)$_m$ concentration in aqueous solutions.

These micelle morphologies were further confirmed by cryo-TEM, as shown in Fig. 7. Due to the negatively staining, the micelles appeared to be bright in the normal TEM images. Whereas, the micelles are black in the cryo-TEM images because of the higher electron density of micelles than that of the surrounding ices at −170 °C. Each micelle morphology shown in Fig. 6 was also observed by cryo-TEM from the identical (PNIPAm-P*t*BA-PNIPAm)$_m$ micelle solution.

The toroid structure 1 (label 1) in Fig. 6A corresponds to the unclosed vesicular structure 1′ (label 1′) in Fig. 7A. Close vesicular-like structures (label 1″) were also observed in Fig. 7A. However, it can be noticed that the cores (or inside) of the vesicular-like structures are not empty, which is quite contrast to the normal vesicles. The wall of vesicular structures can be clearly identified. Interestingly, the electron density of the core was higher than the surround ice and appeared to be light-black, which indicates that there were polymer chains inside the vesicular structures. Such close vesicular structures were observed in (PNIPAm-P*t*BA-PNIPAm)$_m$ aqueous solution with polymer concentration ranging from 0.025 wt.% up to 0.1 wt.% (Fig. 7A, B1, B2, C).

The layer structure 2 (label 2) in Fig. 6A and B were corresponding to the layer structure 2′ (label 2′) in Fig. 7B1. The cryo-TEM image suggests that the stack of the layers is spiral. There is screw dislocation in the four-layer structure. The cage-like structures 3 (label 3) in Fig. 6A and B were also seen in Fig. 7B2 (label 3′). Note that the cage-like structure in Fig. 6A was half-broken.

The spherical micelles (label 4) and their large associated aggregates (label 5) observed in Fig. 6C and D were corresponding to the structure 4′ and 5′ in Fig. 7C and D.

Because of the special chain structure of the linear multiblock copolymer, there are loops of block chains not only in the core but also in the shell of the micelles formed in selective solvent. Special micelle structure may be then expected for multiblock copolymer in selective solvents. For linear multiblock copolymers, theoretical studies predicted that a flower-like single intramolecular micelle or a string of molecular micelles will be formed in selective solvent [28]. Most recently, Hugouvieux et al. performed three-dimensional Monte Carlo simulations on dilute solutions of amphiphilic multiblock copolymers with a large number of blocks, micelles, chains of micelles, tubes, and layered structures were found, which depended on the ratio of hydrophobic to hydrophilic block lengths and the quality of the solvent [32]. Scheme 2 schematically shows the possible micelle structures of linear multiblock copolymer in selective solvent predicted by theory and simulations. Hugouvieux

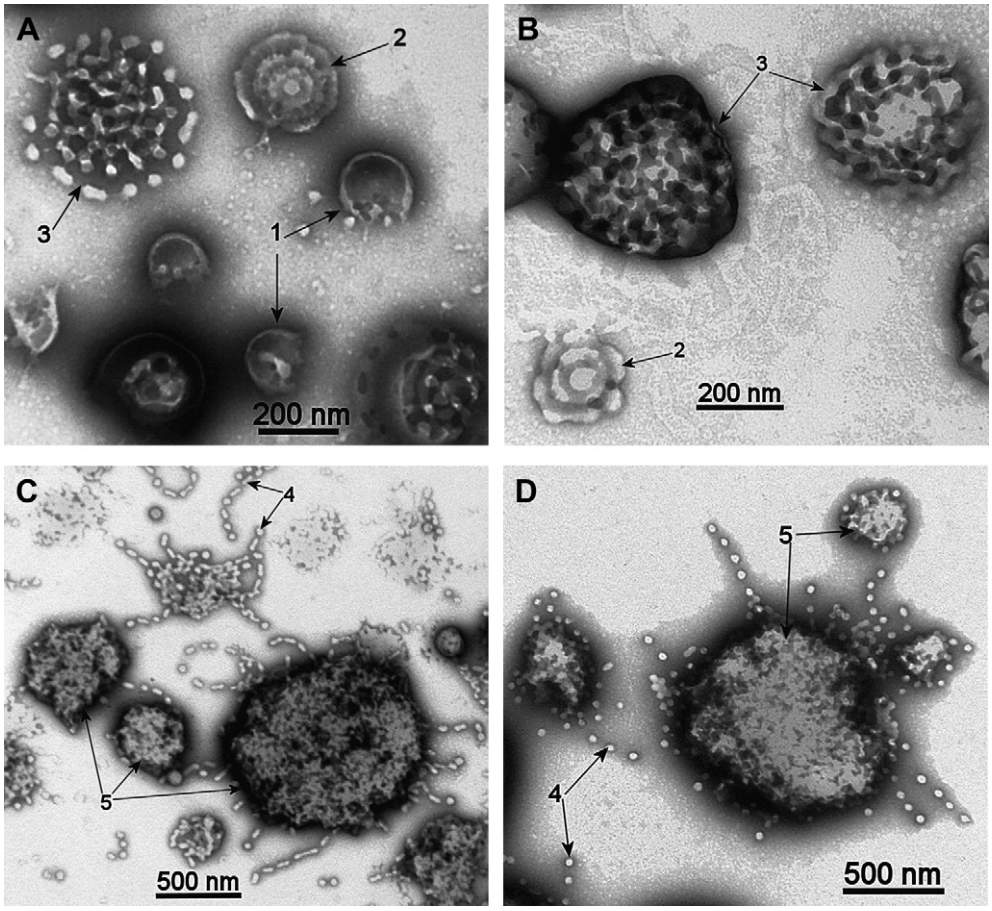

Fig. 6. The normal TEM images of (PNIPAm-P*t*BA-PNIPAm)$_m$ micelles in aqueous solution. The initial concentrations of (PNIPAm-P*t*BA-PNIPAm)$_m$ THF solutions were (A) 0.025 wt.%, (B) 0.05 wt.%, (C) 0.1 wt.%, and (D) 0.25 wt.%, respectively.

et al. [32]. showed that when the hydrophobic substitution rate, $P_{sub} \leq 0.3$, the linear multiblock copolymer chains favor to form intramolecular chains of micelles. The hydrophobic blocks form spherical or ellipsoidal clusters, which are linked to each other by one or several hydrophilic blocks. For $P_{sub} > 0.5$, tubular and layered structure will be formed in selective solvent, which is the very poor solvent for the hydrophobic blocks. Specially, purely energetic considerations suggest that for sufficiently large values of E_i the layered structure is always favored, no matter how long the hydrophilic blocks. Note that the effective energy E_i presents the interaction between neighboring hydrophobic monomers. For increasing E_i, the solvent becomes increasingly poor for hydrophobic monomers. In the present study, the NMR and GPC results show $P_{sub} \sim 0.7$ for (PNIPAm-P*t*BA-PNIPAm)$_m$. Furthermore, the aqueous solution is sufficiently poor for the hydrophobic P*t*BA blocks. Hence, E_i will be sufficiently large for (PNIPAm-P*t*BA-PNIPAm)$_m$ chains in aqueous solution. As the results, (PNIPAm-P*t*BA-PNIPAm)$_m$ chains may be expected to form layered structures in aqueous solutions. The normal TEM and cryo-TEM images show that layered structures are indeed observed, including vesicular structures and spirally stacked layers (cf. Figs. 6 and 7). Spherical and ellipsoidal micelles are also found with higher initial copolymer solutions. These results are in excellent consistent with the prediction of the three-dimensional Monte Carlo simulations.

Furthermore, novel micelle structure, namely net-cage micelle, is also observed in (PNIPAm-P*t*BA-PNIPAm)$_m$ aqueous solutions. Cage-like micelles have been mapped out in a computer simulation study of structure formation in amphiphilic block copolymer solutions after a quench form a homogeneous state [41]. As predicted, complex micelle structures, including ring micelles, toroidal micelles, and cage-like micelles, may be possibly formed when the concentration of the copolymer solution is close to the CMC of the copolymer. The CMC is about 0.014 mg/ml or 0.0014 wt.% for (PNIPAm-P*t*BA-PNIPAm)$_m$ in aqueous solution. The net-cage micelles are experimentally observed here for (PNIPAm-P*t*BA-PNIPAm)$_m$ aqueous solution with 0.05 wt.% (cf. Figs. 6B and 7B2). The intermediate structures of the (PNIPAm-PtBA-PNIPAm)$_m$ micelles during the dialysis process were also investigated by TEM. Figs. S2 and S3 showed that the morphologies of (PNIPAm-P*t*BA-PNIPAm)$_m$ micelles were hardly changed during the dialysis process. The morphology of (PNIPAm-P*t*BA-PNIPAm)$_m$ micelle had little changes and similar with the primary micelles after the micelle solution was first heated up to 50 °C and then cooling from 50 °C back to 10 °C, as shown in Fig. S4 (see Supporting information).

3.4. Light scattering measurement of (PNIPAm-PtBA-PNIPAm)$_m$ micelle in aqueous solution

The ensemble behavior, hydrodynamic diameter, and size distribution of the (PNIPAm-P*t*BA-PNIPAm)$_m$ micelles in aqueous solution were investigated at 25 °C by static and dynamic light scattering (SLS & DLS). Fig. 8A shows the typical normalized squared electric field auto-correlation functions $g_1(\tau)$ obtained by DLS at a scattering angle of $\theta = 90°$ and 25 °C for various (PNIPAm-

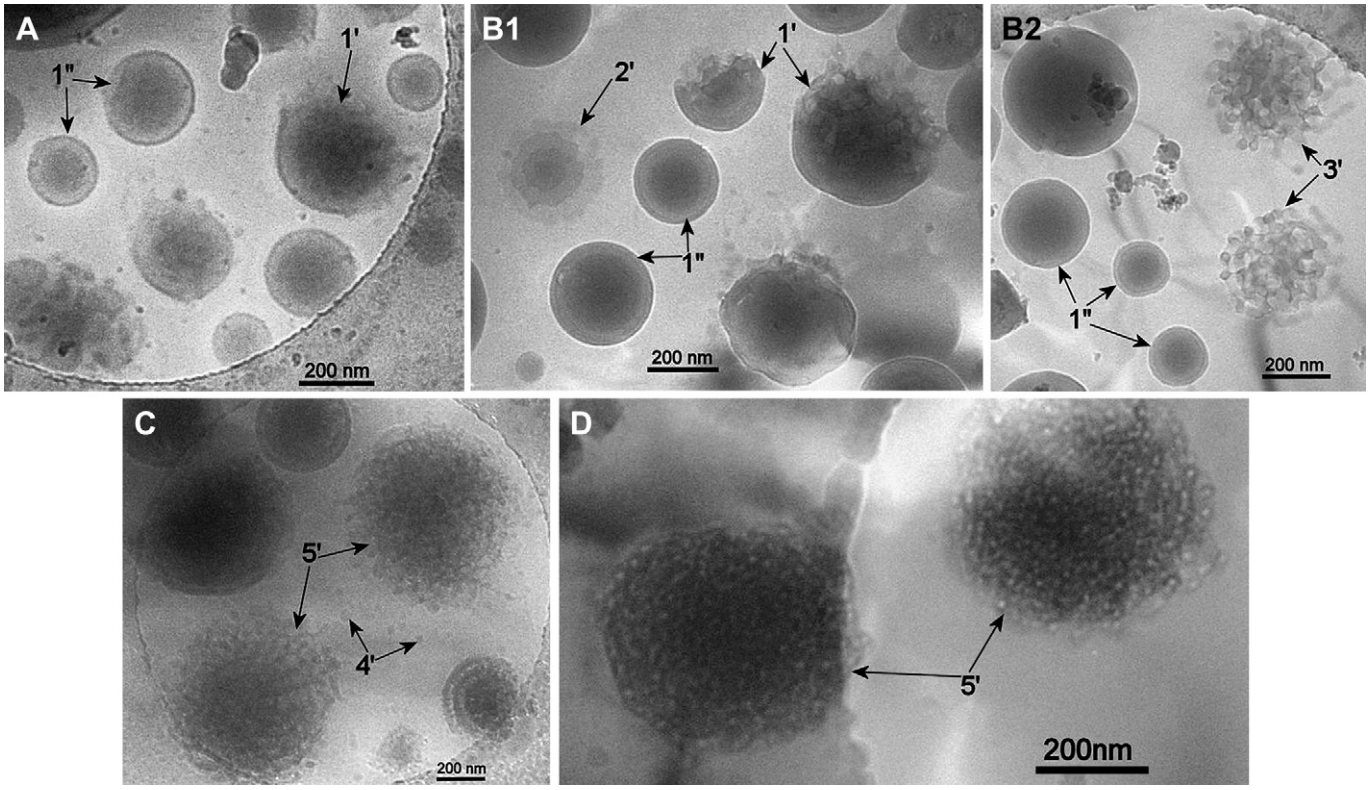

Fig. 7. The cryo-TEM images of (PNIPAm-P*t*BA-PNIPAm)$_m$ micelles in aqueous solution. The initial concentrations of (PNIPAm-P*t*BA-PNIPAm)$_m$ THF solutions were (A) 0.025 wt.%, (B1) 0.05 wt.%, (B2) 0.05 wt.%, (C) 0.1 wt.%, and (D) 0.25 wt.%, respectively.

P*t*BA-PNIPAm)$_m$ micelle solutions. The second-order cumulant expansion was used to fit $g_1(\tau)$, which was given as [42,43].

$$g_1(\tau) = A\exp(-\Gamma\tau)\left(1+\frac{1}{2!}\mu_2\tau^2+\ldots\right) \quad (1)$$

where Γ is the decay rate, and μ_2/Γ^2 characterizes the width of the decay. The solid lines in Fig. 8 indicate that the equation (1) fits the decay curves well, indicating a monomodal size distribution of micelles [42,43]. The inset of Fig. 8A shows the corresponding hydrodynamic diameter, D_h, distribution of the (PNIPAm-P*t*BA-PNIPAm)$_m$ micelles in aqueous solutions calculated by the inverse Laplace transformation with the software package provided by the manufacture. Fig. 8B indicates that the decay rate Γ measured at various scattering angles exhibits excellent linearity versus the square of scattering wavevector q^2. Note that $q=(4\pi n/\lambda)\sin(\theta/2)$ with λ and n being the wavelength of the laser light in vacuum and the refractive index of solvent, respectively. Fig. 8 indicates that the

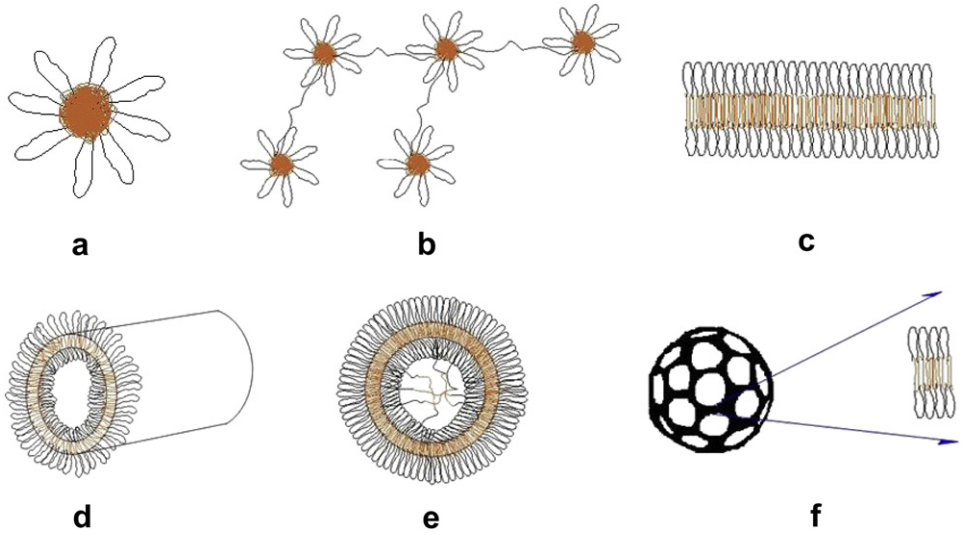

Scheme 2. Possible micelle morphologies of linear multiblock copolymer in selective solvent. (a) single flower micelle, (b) chain of micelles, (c) layered structures, (d) tube, (e) vesicular structure with chains inside, and (f) net-cage-like micelle. Note that micelle structures of (a)–(d) have been predicted by theory and simulations [28,32] whereas micelle structures of (e) and (f) were observed in the present work.

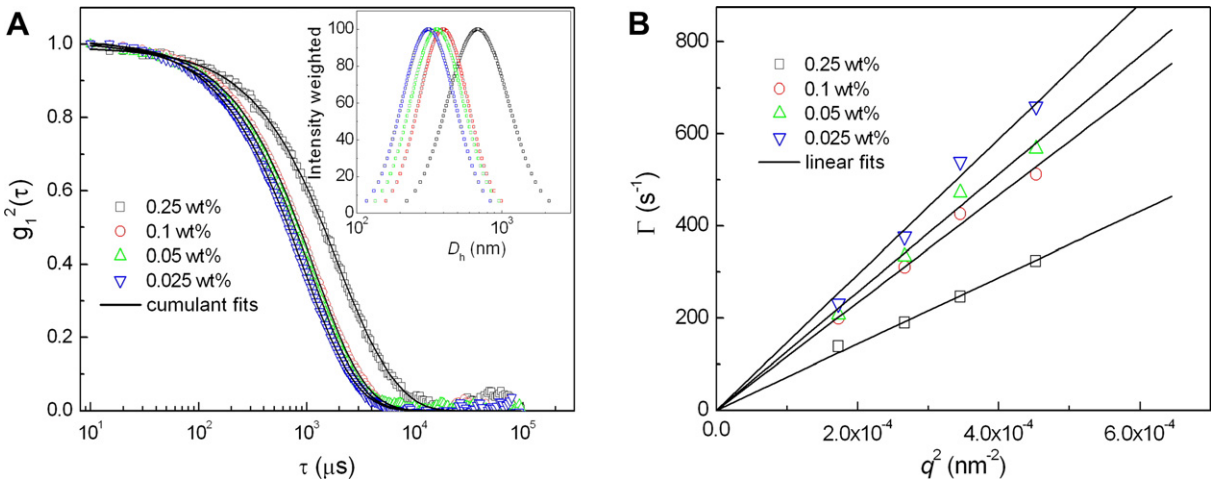

Fig. 8. (A) The normalized squared electric field auto-correlation function $g_1(\tau)$ of (PNIPAm-P*t*BA-PNIPAm)$_m$ micelles in aqueous solutions measured by DLS at $\theta = 90°$ and 25 °C. The solid lines are second-order cumulant fits. The inset shows the corresponding D_h distribution. (B) The decay rate Γ as the function of scattering vector, q and the linear fits of decay rate Γ vs q^2. The initial concentration of (PNIPAm-P*t*BA-PNIPAm)$_m$ THF solution were 0.025 wt.%, 0.05 wt.%, 0.1 wt.%, and 0.25 wt.%, respectively.

size and size distribution of micelles increases with increasing the initial concentration of multiblock copolymer. The hydrohynamic radius R_h of the micelles is about 167 nm, 192 nm, 210 nm, and 341 nm for the micelles prepared from the (PNIPAm-P*t*BA-PNIPAm)$_m$ THF solution with initial concentration of 0.025 wt.%, 0.05 wt.%, 0.1 wt.%, and 0.25 wt.%, respectively. These DLS results are consistent with those obtained by cryo-TEM and normal TEM measurements.

Fig. 9 shows the light scattering intensity I of (PNIPAm-P*t*BA-PNIPAm)$_m$ micelles in aqueous solutions as a function of scattering vector q in log–log scale measured by SLS at 25 °C. A power-law dependence of $I \sim q^{-3.5}$ is found for q ranging from ~0.008 nm to ~0.022 nm. I shows the upturn at higher q. Again, the SLS results agree well with the simulation form factors $F(q)$ of linear amphiphilic multiblock copolymer by Hugouvieux et al. [32]. Note, $F(q)$ gives assessments of the multiscale structures of polymeric micelles in solutions and can be experimentally measured using SLS, neutron, as well as X-ray scattering. In selective solvent, the low q region of form factor, $F(q)$, for $qR_g << 1$, characterizes the overall size of copolymer micelles. In the intermediate q range, for $qR_g \geq 1$, $F(q)$ probes the internal structure of the micelles. Especially, $F(q) \propto q^{-4}$ presents a compact spherical structure. The two-dimensional layer structure of micelle is described by a $F(q) \propto q^{-2}$ behavior. The static light scattering intensity I shown in Fig. 9 is proportional to the form factor $F(q)$ of the (PNIPAm-P*t*BA-PNIPAm)$_m$ micelles in aqueous solutions. With the size of (PNIPAm-P*t*BA-PNIPAm)$_m$ micelles obtained by TEM and DLS, $qR_g \geq 1$ is obviously held for the q range studied here. A power-law dependence of $I \sim q^{-3.5}$ observed here indicates that the (PNIPAm-P*t*BA-PNIPAm)$_m$ micelles is not with compact structures, which is consistent with the results of TEM.

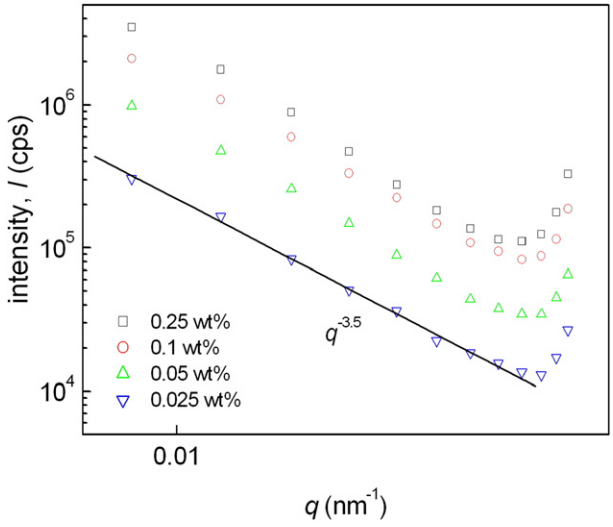

Fig. 9. The light scattering intensity I of (PNIPAm-P*t*BA-PNIPAm)$_m$ micelles in aqueous solutions as a function of scattering vector q in log–log scale measured by SLS at 25 °C. The solid line shows the power-law dependence of $I \sim q^{-3.5}$. The initial concentration of (PNIPAm-P*t*BA-PNIPAm)$_m$ THF solution were 0.025 wt.%, 0.05 wt.%, 0.1 wt.%, and 0.25 wt.%, respectively.

3.5. Thermo-sensitivity of (PNIPAm-PtBA-PNIPAm)$_m$ micelle in aqueous solution

As it is well known, PNIPAm exhibits a lower critical solution temperature (LCST) at~32 °C in aqueous solution [44]. Below LCST, PNIPAm is hydrophilic and soluble in aqueous solution. When increasing the solution temperature above LCST, PNIPAm becomes hydrophobic, insoluble, and aggregates in aqueous solution. For (PNIPAm-P*t*BA-PNIPAm)$_m$ micelles in aqueous solution, the hydrophilic PNIPAm block chains form the corona of the micelles and sterically stabilize the micelles in aqueous solution. Hence, the (PNIPAm-P*t*BA-PNIPAm)$_m$ micelles is expected to exhibit thermo-sensitive behavior in aqueous solution as PNIPAm does. The (PNIPAm-P*t*BA-PNIPAm)$_m$ micelles prepared from the copolymer THF solutions with initial concentrations of 0.025 wt.% and 0.05 wt.% were thus investigated. Fig. 10 shows the hydrodynamic diameters D_h of the (PNIPAm-P*t*BA-PNIPAm)$_m$ micelles in aqueous solutions as a function of temperature measured by dynamic light scattering (DLS) at $\theta = 90°$. The hydrodynamic diameter decreases with increasing the solution temperature from 25 °C to 50 °C. Similar to PNIPAm-containing micelles, both (PNIPAm-P*t*BA-PNIPAm)$_m$ micelles exhibit reversible thermo-sensitive behavior. When the temperature was cooled down to the room temperature, the hydrodynamic diameter of the micelles increases back again. However, large hysteresis was also observed for the micelles prepared from the initial copolymer concentration of 0.05 wt.%. The hysteresis during the heating–cooling cycle can be attributed to the intrachain and interchain interactions formed in the

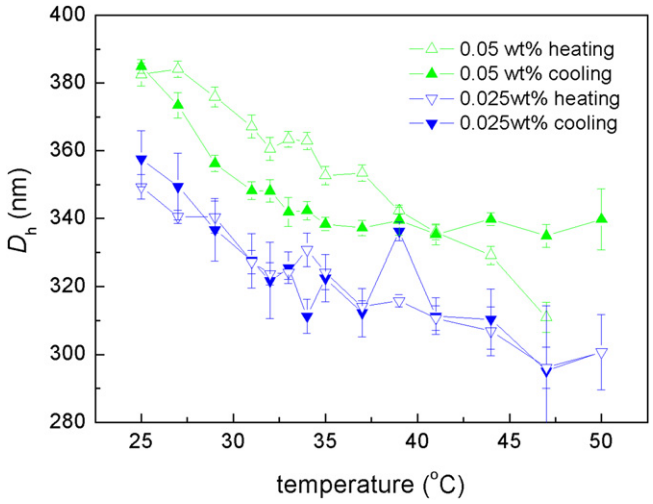

Fig. 10. The hydrodynamic diameter, D_h, of the (PNIPAm-P*t*BA-PNIPAm)$_m$ micelles in aqueous solutions as a function of temperature measured by dynamic light scattering (DLS) at $\theta = 90°$.

collapsed state at high temperature, which will hinder the hydration of the collapsed chains in the cooling process [45–49]. The other possible reason is the difference between the response rate of the (PNIPAm-P*t*BA-PNIPAm)$_m$ micelles and the ramping rate of the temperature, leading to the delay rearrangement of PNIPAm blocks in aqueous solution. In a close related system, Troll et al. [50] observed hysteresis of turbidity of polystyrene-*b*-poly (*N*-isopropylacrylamide) (PS-PNIPAm) micelles in aqueous solution during heating and cooling cycles, while no hysteresis was observed by dynamic light scattering (DLS) when cooling the micelles down from 40 °C. However, above 40 °C, DLS measurements observed the increasing of micelle size, suggesting the association of different collapse micelles [50]. The authors attributed the hysteresis to the difference of temperature ramping rates between turbidimetry and DLS measurements. The (PNIPAm-P*t*BA-PNIPAm)$_m$ micelles were also confirmed to be stable in aqueous solution at 50 °C for at least 48 h, as shown in Fig. S5 (Supporting information). Furthermore, no phase transition temperature can be identified, which is much different to the LCST of PNIPAm and may be attributed to the complicated structure of the (PNIPAm-P*t*BA-PNIPAm)$_m$ micelles and the confinement of PNIPAm blocks in the micelles due to the multiblock chain structure.

4. Conclusion

A linear amphiphilic multiblock copolymer (PNIPAm-P*t*BA-PNIPAm)$_m$ was successfully synthesized by a two-step reversible addition–fragmentation transfer (RAFT) polymerization in the presence of a cyclic trithiocarbonate as RAFT agent. The ratio of the monomer numbers of P*t*BA blocks and PNIPAm blocks was about 2.2 determined by NMR. The average value of *m* was about 3.6 with a polydispersity of 1.96. The micelle behavior of (PNIPAm-P*t*BA-PNIPAm)$_m$ multiblock copolymer in aqueous solution was then investigated by means of normal TEM, cryo-TEM, static and dynamic light scattering. Self-consistent results were obtained by different techniques. The morphology, size, and size distribution of (PNIPAm-P*t*BA-PNIPAm)$_m$ micelles were found to be dependent on the initial concentration of multiblock copolymer in THF. Spherical micelles, associated aggregates of spherical micelles, layered structures, and vesicular micelles were experimentally observed, which were in good agreement with the prediction of simulations on linear amphiphilic multiblock copolymer in selective solvent. New morphology of net-cage micelles was also observed. A power-law dependence of $I \sim q^{-3.5}$ was observed by static light scattering, indicating that the (PNIPAm-P*t*BA-PNIPAm)$_m$ micelles is not with compact structures. Rendering from the character of PNIPAm blocks, the (PNIPAm-P*t*BA-PNIPAm)$_m$ micelles also exhibit thermo-sensitive behavior in aqueous solution. Such preliminary studies may further evoke more interests and experimental investigation in the solution behavior of linear amphiphilic multiblock copolymer in selective solvent.

Acknowledgement

We thank the National Natural Science Foundation of China (20604022, 20874087, 20774079) and the Zhejiang Provincial Natural Science Foundation of China (Y406029) for financial support. We thank Prof. Qiang Zheng and Dr. Yonggang Shangguan for the use of BI-200SM.

Appendix A. Supplementary material

Supplementary data associated with this article can be found, in the online version, at doi:10.1016/j.polymer.2010.06.007.

References

[1] Riess G. Prog Polym Sci 2003;28:1107.
[2] Zhulina EB, Adam M, LaRue I, Sheiko SS, Rubinstein M. Macromolecules 2005;38:5330.
[3] Zhu JT, Yu HZ, Jiang W. Eur Polym J 2008;44:2275.
[4] Li XJ, Deng MG, Liu Y, Liang HJ. J Phys Chem B 2008;112:14762.
[5] Parry AL, Bomans PHH, Holder SJ, Sommerdijk N, Biagini SCG. Angew Chem Int Ed 2008;47:8859.
[6] Pham TT, Pattanayek SK, Pereira GG. J Chem Phys 2005;123:12.
[7] Du BY, Mei AX, Yin KZ, Zhang QF, Xu JT, Fan ZQ. Macromolecules 2009;42:8477.
[8] Tung PH, Kuo SW, Chen SC, Lin CL, Chang FC. Polymer 2007;48:3192.
[9] Chen ZY, Cui HG, Hales K, Li ZB, Qi K, Pochan DJ, et al. J Am Chem Soc 2005;127:8592.
[10] Yu GE, Eisenberg A. Macromolecules 1998;31:5546.
[11] Choucair A, Lavigueur C, Eisenberg A. Langmuir 2004;20:3894.
[12] Cui HG, Chen ZY, Wooley KL, Pochan DJ. Macromolecules 2006;39:6599.
[13] Du HB, Zhu JT, Jiang W. J Phys Chem B 2007;111:1938.
[14] LaRue I, Adam M, Pitsikalis M, Hadjichristidis N, Rubinstein M, Sheiko SS. Macromolecules 2006;39:309.
[15] Reynhout IC, Cornelissen J, Nolte RJM. J Am Chem Soc 2007;129:2327.
[16] Choucair A, Eisenberg A. Eur Phys J E 2003;10:37.
[17] Azzam T, Eisenberg A. Angew Chem Int Ed 2006;45:7443.
[18] Terreau O, Luo LB, Eisenberg A. Langmuir 2003;19:5601.
[19] Jiang Y, Zhu JT, Jiang W, Liang HJ. J Phys Chem B 2005;109:21549.
[20] Pochan DJ, Chen ZY, Cui HG, Hales K, Qi K, Wooley KL. Science 2004;306:94.
[21] Hadjiantoniou NA, Triftaridou AI, Kafouris D, Gradzielski M, Patrickios CS. Macromolecules 2009;42:5492.
[22] Zhang Q, Ye J, Lu Y, Nie T, Xie D, Song Q, et al. Macromolecules 2008;41:2228.
[23] Hong LZ, Zhu FM, Li JF, Ngai T, Xie ZW, Wu C. Macromolecules 2008;41:2219.
[24] Determan MD, Guo L, Thiyagarajan P, Mallapragada SK. Langmuir 2006;22:1469.
[25] Zhou YM, Jiang KQ, Song QL, Liu SY. Langmuir 2007;23:13076.
[26] Sommerdijk N, Holder SJ, Hiorns RC, Jones RG, Nolte RJM. Macromolecules 2000;33:8289.
[27] Jia ZF, Xu XW, Fu Q, Huang JL. J Polym Sci Polym Chem 2006;44:6071.
[28] Halperin A. Macromolecules 1991;24:1418.
[29] Zhang GZ, Winnik FM, Wu C. Phys Rev Lett 2003;90:035506.
[30] Lintuvuori JS, Wilson MR. Phys Chem Chem Phys 2009;11:2116.
[31] Gindy ME, Prud'homme RK, Panagiotopoulos AZ. J Chem Phys 2008;128:164906.
[32] Hugouvieux V, Axelos MAV, Kolb M. Macromolecules 2009;42:392.
[33] Lei P, Wang Q, Hong J, Li YX. J Polym Sci Polym Chem 2006;44:6600.
[34] Hong J, Wang Q, Lin YZ, Fan ZQ. Macromolecules 2005;38:2691.
[35] Hong J, Wang Q, Fan ZQ. Macromol Rapid Commun 2006;27:57.
[36] Zhang LS, Wang Q, Lei P, Wang X, Wang CY, Cai L. J Polym Sci Polym Chem 2007;45:2617.
[37] Wilhelm M, Zhao CL, Wang YC, Xu RL, Winnik MA, Mura JL, et al. Macromolecules 1991;24:1033.
[38] Minatti E, Viville P, Borsali R, Schappacher M, Deffieux A, Lazzaroni R. Macromolecules 2003;36:4125.
[39] Zhang LF, Eisenberg A 2nd International symposium on molecular order and mobility in polymer systems. St Petersburg, Russia; 1996. p. 221.
[40] Zhang LF, Eisenberg A. Polym Adv Technol 1998;9:677.

[41] He X, Schmid F. Phys Rev Lett 2008;100:137802.
[42] Zhang LF, Barlow RJ, Eisenberg A. Macromolecules 1995;28:6055.
[43] He YY, Li ZB, Simone P, Lodge TP. J Am Chem Soc 2006;128:2745.
[44] Schild HG. Prog Polym Sci 1992;17:163.
[45] Liu GM, Cheng H, Yan LF, Zhang GZ. J Phys Chem B 2005;109:22603.
[46] Wu C, Zhou SQ. Macromolecules 1995;28:5388.
[47] Wu C, Zhou SQ. Phys Rev Lett 1996;77:3053.
[48] Cao Z, Du BY, Chen TY, Li HT, Xu JT, Fan ZQ. Langmuir 2008;24:5543.
[49] Plunkett MA, Wang ZH, Rutland MW, Johannsmann D. Langmuir 2003;19:6837.
[50] Troll K, Kulkarni A, Wang W, Darko C, Koumba AMB, Laschewsky A, et al. Colloid Polym Sci 2008;286:1079.